Antiferromagnetism in UO_2 thin epitaxial films

Z. Bao,[1] R. Springell,[2] H. C. Walker,[3,*] H. Leiste,[4] K. Kuebel,[4] R. Prang,[4] G. Nisbet,[5] S. Langridge,[6] R. C. C. Ward,[7] T. Gouder,[1] R. Caciuffo,[1] and G. H. Lander[1]

[1]*European Commission, Joint Research Centre, Institute for Transuranium Elements, Postfach 2340, D-76125 Karlsruhe, Germany*

[2]*Royal Commission for the Exhibition of 1851 Research Fellow, Interface Analysis Centre, School of Physics, University of Bristol, Bristol BS2 8BS, United Kingdom*

[3]*European Synchrotron Radiation Facility (ESRF), Boîte Postale 220, F-38043 Grenoble, France*

[4]*Karlsruhe Institute of Technology KIT, Institute for Applied Materials (IAM-AWP), Hermann-von-Helmholtz-Platz 1, 76344 Eggenstein-Leopoldshafen, Germany*

[5]*Diamond Light Source Ltd., Diamond House, Harwell Science and Innovation Campus, Didcot, Oxfordshire OX11 0DE, United Kingdom*

[6]*ISIS, Rutherford Appleton Laboratory, Harwell Science and Innovation Campus, Oxon OX11 0QX, United Kingdom*

[7]*Clarendon Laboratory, University of Oxford, Oxford, Oxon OX1 3PU, United Kingdom*

(Received 9 June 2013; revised manuscript received 25 August 2013; published 25 October 2013)

Thin films (250–4500 Å) of epitaxial UO_2 were produced by reactive sputtering on two different substrate materials: $LaAlO_3$ and CaF_2. Using the large enhancement present with resonant x-ray scattering using photons at the uranium M_4 absorption edge, antiferromagnetic (AF) order was found in all films. The ordering temperature T_N is the same as the bulk, but the films show second-order (continuous) transitions in contrast to the first-order bulk transition. For $LaAlO_3$-based films, an additional strong diffuse magnetic disorder is observed, which is reminiscent of the second-length scale, associated with structural disorder and/or strain. By using a formulation accounting for the strong absorption and coherent nature of the photons, the energy widths at the U M_4 resonances can be related to the thickness of the AF region. The $LaAlO_3$-based films do not order magnetically over more than ∼600 Å, whereas the CaF_2-based film orders throughout. Further, for thicker films (>1000 Å) the fitting procedure shows that the AF order is located at the top of the $LaAlO_3$-based film. This points to the formation in thicker films of a nonmagnetic layer of UO_2 adjacent to the substrate, which may have tetragonal symmetry.

DOI: 10.1103/PhysRevB.88.134426 PACS number(s): 75.80.+q, 77.65.−j

I. INTRODUCTION

The production of epitaxial films of UO_2 has a number of possible applications, especially those in optics and nuclear-related studies. Early investigations in both of these fields were undertaken with polycrystalline films;[1–5] however, more recently epitaxial films on various substrates have been synthesized.[6–8] These can allow further studies compared to those possible with polycrystalline films; for example, the study of electronic structure with angular-resolved photoemission spectroscopy (ARPES), surface and near-surface antiferromagnetism (AF) by resonant x-ray scattering (RXS), the study of electrochemical effects on the surface of UO_2 via the technique of grazing-incidence x-ray diffraction (GIXRD), and the study of neutron damage by simulating it with heavy-ion bombardment. An advantage of epitaxial films is that the surfaces can be made of different U-O stoichiometries, which cannot be produced in bulk single-crystal form, as demonstrated in Ref. 6. Additionally, since the production of thin films requires a substrate, one can control growth parameters such as the substrate, buffer layer, gas pressure, and substrate temperature to engineer crystallographic structure, the orientation of the film, strain fields, and even the stoichiometry in epitaxial single-crystal layers. This paper is concerned with the interplay between the film structure and dimensionality, and the manifestation of antiferromagnetic order.[9] If production of such epitaxial films can be extended into transuranium materials, this opens the possibility of advanced physics and chemistry experiments on small amounts of radioactive material. For example, an epitaxial film of 250 Å thickness and a surface area of 1 × 1 cm^2 of an actinide oxide contains only ∼20 μg of actinide material.

The present study concerns principally the magnetism of thin films of UO_2 via RXS studies. UO_2 orders in a 3**k** type-I antiferromagnetic (AF) structure (T_N) at 31 K, and, in its bulk form, has been studied in great detail for the past 45 years.[10] Moreover, RXS was used more than a decade ago to investigate the near-surface[11] and surface[12,13] behavior of the magnetism of UO_2 bulk single crystals. Pertinent questions addressed by the present study are the behavior of T_N as a function of film thickness t, and whether the magnetism in the films shows the unusual surface melting and the suppression of long-range order, termed a "dead" layer, that can be found on the surface of a bulk crystal.[12,13]

II. PRODUCTION AND CHARACTERIZATION OF FILMS

All samples studied in this work were prepared by reactive (-gas) sputtering with deposition temperatures of ∼650 °C.[7,8] The majority were prepared at ITU, Karlsruhe, on commercially available (001) substrates of $LaAlO_3$ with a Mg cap of ∼500 Å. $LaAlO_3$ has a perovskite (pseudocubic Pm-$3m$) structure with $a_0 = 3.791$ Å at room temperature. As described in Ref. 8, the epitaxial relationship is with cubic UO_2 ($a_0 = 5.469$ Å, at room temperature) rotated 45° around the [001] surface normal so that the (110) plane of UO_2, with a d-spacing of $a_0/\sqrt{2} = 3.867$ Å, fits with the $LaAlO_3$ (100) plane, with a d-spacing of 3.791 Å. This causes the UO_2 to be in compression of −2.0% with respect to the substrate in-plane spacing. A final sample of nominal

TABLE I. Details of the samples used. All samples are on $LaAlO_3$ substrates, except D18, which is on CaF_2. Mg caps were ~500 Å, and the Nb cap was 250 Å. Nominal film thickness, estimated from deposition rate, is given by t_{nom}. The x-ray reflectivity (XRR) gives the thickness (1–2%) (for $t < 1000$ Å), and the mean-square roughness σ for all samples is 6 ± 2 Å. The crystal lattice parameters (± 0.005 Å) of the film are given by c (out-of-plane) and a (in-plane) dimensions measured at room temperature. The rocking curve width (FWHM $\pm$ 0.1°) is for the charge (002) reflection, except for sample D18, where it is the magnetic (001) reflection; $\Delta\omega$ is given in degrees.

Sample	Cap.	t_{nom} (Å)	t_{XRR} (Å)	c (Å)	a (Å)	$\Delta\omega$ (deg)
S02	Mg	80	76	5.541		2.4
S03	Mg	150	136	5.520	5.394	1.9
S04	Mg	200	181	5.518	5.415	1.8
D11	Mg	250	244	5.502	5.422	1.3
S05	Mg	400	398	5.499	5.442	1.2
S06	Mg	550	554	5.490	5.444	1.0
S07	Mg	850	821	5.487	5.446	0.9
D14	Mg	1250				0.9
D15	Mg	2250		5.487	5.445	0.9
D17	Mg	4500				0.9
D18	Nb	2000				0.16

thickness ~2000 Å was grown at Bristol University, with the sputtering apparatus formerly at the University of Oxford.[7,14] The substrate was CaF_2 (100) which has a lattice parameter of $a_0 = 5.451$ Å and an identical crystal structure to UO_2. The subsequent in-plane strain is -0.3%, and thus considerably less than when using $LaAlO_3$. This film was capped with 250 Å of Nb. This thin-film sample cannot be characterized with x-ray diffraction at ambient temperature as the UO_2 and CaF_2 reflections completely overlap. The mosaic listed in Table I is therefore of the magnetic (001) reflection below T_N.

A first question with the reactive-gas sputtering technique is the partial pressure of oxygen needed to grow stoichiometric UO_2. Here the ITU apparatus has an advantage over other reported efforts, as the films are grown in a chamber fully equipped with photoemission capabilities, both in the UPS and XPS regions.[15] We show in Fig. 1 the result of *in situ* studies of the spectra as the partial pressure is changed. This shows that partial pressures of 10^{-6} mbar (10^{-4} Pa) are required to make stoichiometric UO_2, in agreement with the values determined in Refs. 2, 3, and 7. At this partial pressure there is no longer any weight at the Fermi level in the UPS spectra [see Fig. 1(a)].

Atomic force microscopy (AFM) was used to characterize the surface quality, and the results are shown in Fig. 2. As expected, the polished $LaAlO_3$ is smooth [Fig. 2(a)], whereas the UO_2 grown on this substrate [Fig. 2(b)] appears to have regular waves on a scale of ~300 nm in-plane. One would have to measure off-specular reflectivity to model this in-plane roughness more precisely. As measured from the specular reflectivity, the roughness was 6 ± 2 Å. The Mg cap, which has a thickness of ~500 Å, has a much greater roughness of about 55 Å, as measured by x-ray reflectivity, and this clearly conforms to the visual impression in Fig. 2(c). Cross-sectional transmission electron microscopy (TEM) of these samples

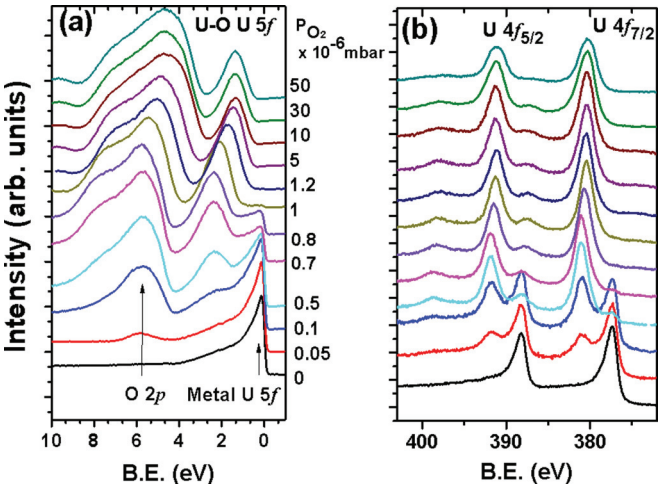

FIG. 1. (Color online) Evolution of photoelectron spectra as a function of the O_2 pressure. (a) U $5f$ and O $2p$ UPS spectra obtained from the radiation source of He I UV light. (b) U $4f$ XPS spectra obtained from Mg $K\alpha$ x-ray radiation.

indicates a relatively good interface between the substrate and UO_2, as was found in Ref. 6.

The films were also examined by x-ray diffraction and reflectivity, both of which are described for such films in Ref. 8. The reflectivity gives the thickness of the films (provided they are less than ~1000 Å) and the roughness, given in Table I. Reciprocal-space mapping (RSM)[16] using x-ray diffraction gives more precision on measuring both the out-of-plane lattice parameter (defined here by c) and, by measuring the

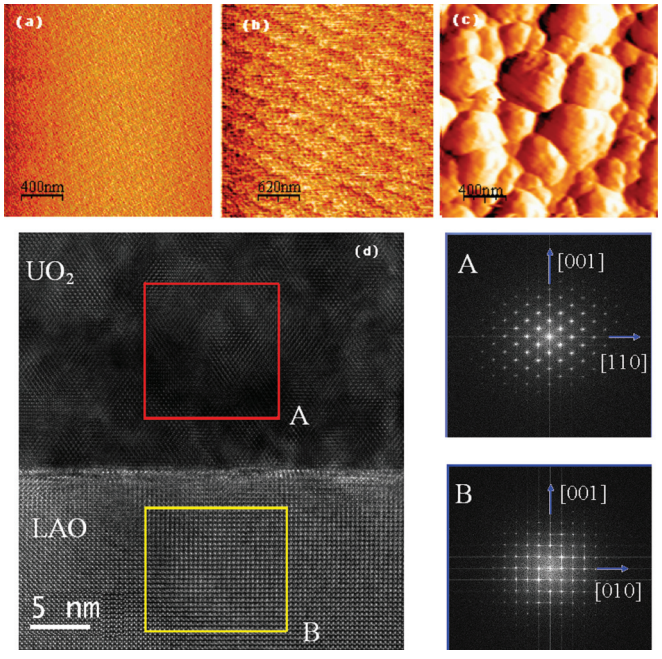

FIG. 2. (Color online) The atomic force microscopy images of (a) $LaAlO_3$ substrate surface, (b) UO_2 film surface, and (c) Mg capping layer surface. Panel (d) presents a TEM image showing the registry between UO_2 and $LaAlO_3$ layers. To the right of this panel are Fourier transforms of the regions A and B with high-symmetry crystallographic orientations labeled.

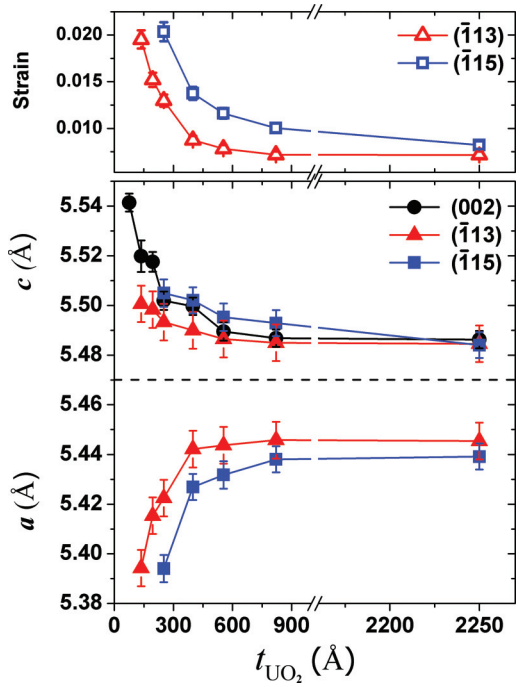

FIG. 3. (Color online) Evolution of the out-of-plane, c, and the in-plane, a, lattice parameters determined from RSM measurements. The dashed line is the bulk value of a and c. The upper panel shows the strain, determined as $(c-a)/(c+a)/2$.

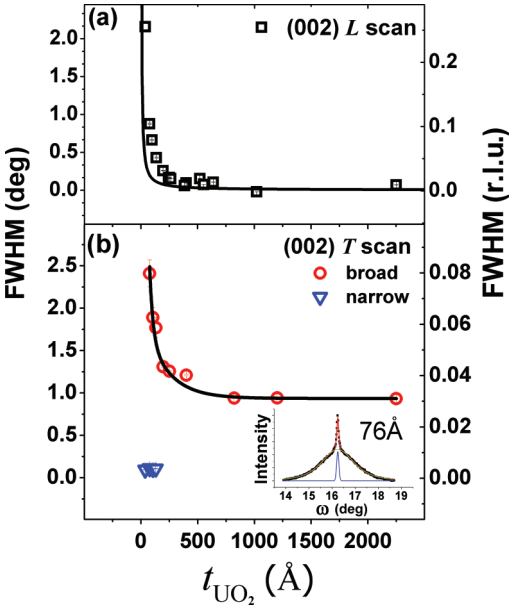

FIG. 4. (Color online) Evolution of the FWHM as a function of the film thickness. (a) (002) peak from L scans. The solid line is a fit using the Scherrer equation. (b) (002) peaks from rocking curve T scans. The solid line is a guide to the eye (exponential decay). The inset shows the rocking curve of a 76 Å film.

off-specular reflections, the in-plane lattice parameter (defined here by a). These are given in Table I, and the a and c lattice parameters are plotted as a function of film thickness in Fig. 3.

For film thicknesses $\leqslant$ 600 Å, Fig. 3 shows that the strain is considerable in the films, and that they are quite far from cubic, with the strain attaining a value of 0.026 for the thinnest films. The difference in-plane between $LaAlO_3$ ($a = 3.791$ Å) and UO_2 ($a/\sqrt{2} = 3.867$ Å) infers a compressive strain on the in-plane structure of UO_2 of -0.020, so that the results in Fig. 3 are a direct result of the mismatch between the substrate and the UO_2. However, perhaps even more surprising is that, although the strain drops by almost a factor of 4, to 0.007 by a film thickness of $\sim$1000 Å, the strain does not reduce further for thicker films of up to 4500 Å. The symmetry of UO_2 remains tetragonal even for films approaching half a micron in thickness.

X-ray diffraction (conventional Cu $K\alpha$ source with samples at room temperature) was used to measure the scattering profile of the (002) charge peak for all $LaAlO_3$-based films. The results for the longitudinal (coupled θ-2θ scans or longitudinal L scans in the notation of this paper) and transverse (so-called rocking scans or T scans) are shown in Fig. 4. In the longitudinal direction [Fig. 4(a)] the widths follow a Scherrer-like[16] behavior (i.e., reflecting the finite size of the thickness, t, of the film in the longitudinal direction). Reciprocal-lattice units in the figure are based on $d^*(001)(\text{r.l.u.}) = 1/c$ (Å^{-1}), where c is the lattice parameter.

Figure 4(b) represents the transverse scan, with the inset showing data for the thinnest film of 75 Å. In these cases, we come across an aspect studied extensively for thin films, namely a sharp and broad component of the scattering. This subject has been discussed at length.[17,18] Although earlier work suggested that these two contributions came from physically different parts of the sample, the weight of evidence supports a model proposed by Wölfing *et al.*[19] in which both components of the scattering come from all the sample volume. There is still a difference in the perfection of the crystals as a function of growth direction, but it is not correct to assign the sharp component to a part of the film near the substrate. Durand *et al.*[20] have also analyzed in more detail data taken from ZnO films on c-Al_2O_3. However, the data available from such studies far exceed what we have accumulated on our samples, and our analysis is therefore less complete. This is particularly true of the data taken using magnetic scattering, where the number of reflections examined is severely limited by working at the U M_4 resonant energy, which corresponds to an x-ray wavelength of 3.364 Å. Only a single specular reflection, the (001), can be accessed. The sharp component can be seen in diffraction patterns of the films up to 200 Å thick, but it only dominates the rocking curves for films up to $\sim$80 Å. A similar situation was considered by Strehle *et al.*,[8] who used r-Al_2O_3 rather than $LaAlO_3$ as a substrate, but the authors did not examine thin enough UO_2 films to see the sharp component (see Table I and Fig. 4 of their paper). However, in the case of UO_2/YSZ, in which Strehle *et al.*[8] found much better films, i.e., a much smaller mosaic in the transverse direction, as determined by rocking curves of $< 0.20^\circ$, the sharp component could still be seen in films of $\sim$800 Å. This result is surprising considering the large lattice mismatch ($\sim$6%) in the UO_2/YSZ system.

There are further difficulties of working with $LaAlO_3$ substrates. It is known that this material has a ferroelastic transition at 560 °C.[21] Some consequences of this transition are

discussed by Lehmann *et al.*,[22] and it seems highly probable that the large mosaic spread found in UO_2 films grown on $LaAlO_3$ substrates (see Table I) is a result of the ferroelastic transition that occurs in the substrate after the films are grown on the heated substrates and then cooled through the transition. Similar large mosaics have been found in earlier UO_2 films made on $LaAlO_3$.[6,7] Finally, we emphasize the importance of the final film (D18) listed in Table I, fabricated at Bristol using UO_2/CaF_2. This film is impossible to characterize with x-ray diffraction at room temperature as all UO_2 and CaF_2 peaks overlap, so any scans see only the dominant scattering from the substrate. However, at low temperature below T_N and with photons tuned to the uranium M_4 resonance, additional magnetic Bragg peaks arise from the antiferromagnetism of UO_2. The (001) magnetic peak has a rocking-curve width of 0.16°, which is only slightly wider than those of the CaF_2 substrate. This is clearly a *much* better sample than any made on $LaAlO_3$ substrates.

III. STUDIES OF ANTIFERROMAGNETISM IN UO_2 THIN FILMS

In the bulk form, UO_2 is known to order in a 3**k** type-I arrangement of moments, with a first-order discontinuous phase transition at $T_N = 31$ K.[10] In this type of antiferromagnetic order, new Bragg peaks are observed at the positions of (*HKL*) in the reciprocal lattice that have *mixed* indices, as opposed to the fcc crystal structure that gives rise to peaks with only all odd or all even *H*, *K*, and *L*. The strongest antiferromagnetic intensity for resonant x-ray scattering occurs at the position (001), since UO_2 has the so-called transverse 3**k** AF structure.[23] In addition to the magnetic Bragg peaks indicating a new periodicity with respect to the magnetic ordering, there is the ordering of the electric quadrupoles in UO_2, which also occurs at T_N.[23] Associated with the ordering of these electric quadrupoles is an internal (charge) distortion of the oxygen cage around each U atom in such a way as to accommodate the changing shape of the electric quadrupoles at the U site, but also retaining the overall cubic symmetry.[23,24] It is this overall cubic symmetry that is closely associated with the 3**k** type of magnetic ordering.

We thus expect synchrotron x-ray scattering from the films cooled to below 30 K to reveal *three* effects.[23] First, at the U M_4 resonance (3.726 keV) photon energy there should be a magnetic peak at (001) and other mixed *HKL* reflections. Second, we should see scattering from the distorted oxygen cage that is similar to a Jahn-Teller (JT) effect, which occurs also at some of the mixed index reflections.[24] This latter effect can be observed at all energies, as it is nonresonant. Separating these effects requires the use of two different energies, one at the U M_4 resonant energy, and the other away from it. Third, RXS scattering can be observed from the quadrupoles directly at the U M_4 resonant energy, but to distinguish these effects from the resonant magnetic scattering, the polarization of the scattered photon beam must be analyzed.[23] Moreover, it occurs at only certain *HKL* values[23] and is much weaker than the pure magnetic (dipole) scattering. To avoid this complication, we have used photons on resonance to observe the magnetic scattering at places where the quadrupole scattering is forbidden (e.g., the specular {001} reflections),

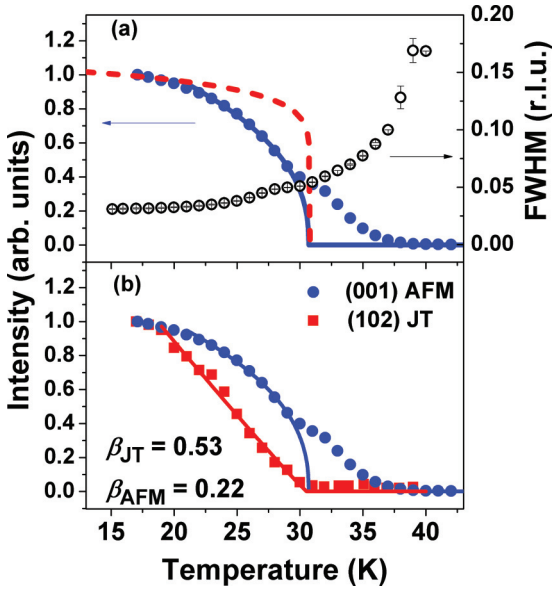

FIG. 5. (Color online) Temperature dependence of the magnetic scattering from D12 (480 Å). (a) Blue points represent the intensity of the (001) magnetic peak measured at U M_4 edge; the blue solid line is the power-law fit to give β. The red dashed line represents the bulk (001) intensity. Black open circles show the FWHM of the transverse (T) scan in r.l.u. (b) Comparison between the temperature dependences of the (001) magnetic and (102) JT peaks measured at incident energies of 3.726 and 5 keV, respectively.

and photons of energies ~5 keV to observe the JT scattering. However, such JT scattering is weaker than the RXS from the magnetic ordering, principally because it involves the oxygen atoms only. Experiments were conducted initially at the ID20 beamline[25] of the European Synchrotron Radiation Facility (ESRF, Grenoble, France) and then at the I16 beamline at the Diamond Synchrotron (Harwell, UK). Closed-cycle displex cryostats were used with base temperatures of 17 and 12 K, respectively.

Figure 5 shows the intensity measured as a function of temperature from sample D12 of a nominal 480 Å thickness. Below T_N the intensity grows according to the power law $I(T)/I(T_0) \approx (1 - T/T_N)^{2\beta}$, where $I(T_0)$ is the intensity at base temperature, and fitting the data allows a determination of β_{AFM} and T_N. In the determination of beta, we have weighted the data near Tn, but we restricted our analysis to two significant numbers, recognizing the difficulty of such analyses. Beta here will be an average (italics) over the film thickness. For surfaces and thin films, beta is known to vary widely, and such changes were already reported for UO_2 surfaces in Ref. 11. There are a number of points to note from Fig. 5:

(i) The transition at ~31 K is not discontinuous (first order), as found in the bulk and shown by the dashed (red) line in frame (a). Instead the transition is strongly second-order with $\beta_{AFM} = 0.22$.

(ii) The diffuse transverse (T) scattering broadens very strongly above T_N, such that the correlation lengths are reduced by about a factor of 4 at $T = 1.2 \times T_N$, but the scattering is still visible. The longitudinal scans were not taken during this experiment.

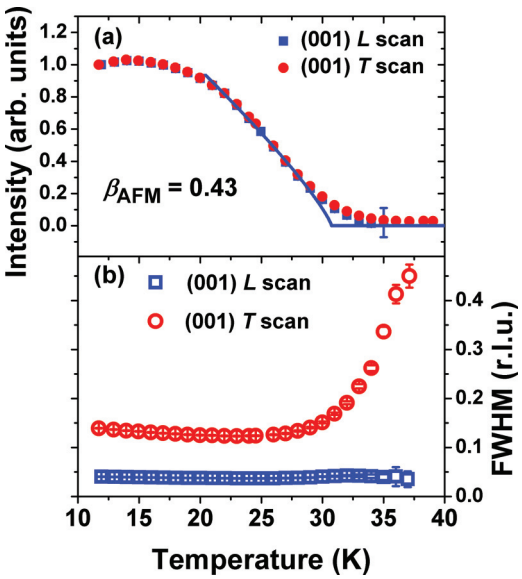

FIG. 6. (Color online) Longitudinal (L) and transverse (T) scans of (001) from D17 (4500 Å). (a) Integrated intensity, (b) FWHM.

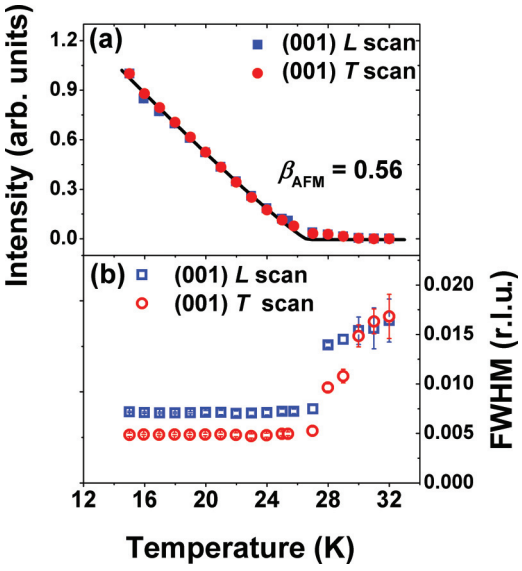

FIG. 7. (Color online) L and T scans of (001) reflections from D18 as a function of temperature (a) Integrated intensity. The solid line is a fit to $\beta_{AFM} = 0.56$. (b) FWHM.

(iii) In frame (b) the Jahn-Teller peak is also shown to be second-order in nature, but is an induced effect as $\beta_{JT} \sim 2\beta_{AFM}$. No critical (charge) scattering appears associated with the disappearance of the JT peak. The Jahn-Teller scattering is much weaker than the magnetic scattering, and at the (102) reflection it can be identified only by moving away from the resonance energy. The scans in Fig. 5(b) were performed with 5 keV photons.

In subsequent experiments, mainly at I16 (Diamond), we performed longitudinal (L) scans as a function of temperature to test whether the strong diffuse scattering near and above T_N was anisotropic in nature. This is illustrated in Fig. 6, which is of the D17 sample with a nominal thickness of 4500 Å. There is a strong divergence of the in-plane correlation length near T_N, with considerable diffuse magnetic scattering seen above T_N. However, in the longitudinal direction, along the growth axis [001] of the thin film, such a divergence is not observed. Such anisotropic critical scattering was present for all films based on $LaAlO_3$ substrates.

In contrast, Fig. 7 shows the scattering from D18, the film based on a CaF_2 substrate. Note that T_N of this film is reduced to ~27 K. We ascribe this to nonstoichiometry, probably a slight excess of oxygen. With this film, we still observe a β value very different from that from a first-order phase transition, as found in bulk UO_2 with $\beta \sim 0$, but there is *no large anisotropy* in the critical scattering near T_N.

Formally, we cannot determine the individual contributions to the ω-scan (transverse) FWHMs unless a number of different reflections are examined.[16] The main contributions will almost certainly be, first, the intrinsic mosaic width of the crystallite blocks making up the film (which should be independent of temperature), and, second, the finite correlation lengths of the scattering from individual crystalline blocks. The first contribution from the mosaic will be independent of the scattering vector, whereas the second effect, due to finite correlation lengths, represents a fixed length in reciprocal space, so its contribution to the measured mosaic width depends inversely on the length of the scattering vector. In the case of the magnetic scattering, we are limited to the (001) reflection along the specular direction because of the long wavelength of the x rays at the U M_4 resonant energy. As a starting assumption, therefore, we take the transverse scans of the (002) charge reflection (see Table I and Fig. 4) as a measure of the mosaic crystal structure. For films thicker than ~800 Å this appears to saturate at 0.9°. In performing the transverse scans of the magnetic (001) reflection, we then assume that any *additional* width is caused by the finite *magnetic* correlations. Provided that these effects can be represented by Gaussian distributions, they add in quadrature,[16] so we can have an approximate measure of the *magnetic* correlation lengths in the plane of the film, especially when the magnetic FWHM values are considerably greater than that of the (002) charge reflections. To convert the widths from FWHM degrees to r.l.u., we have assumed that the contributions are due to a reduced *magnetic* correlation length.

For the D17 sample we observe a FWHM of 3.74° of the magnetic (001) peak, whereas the corresponding charge peak has a FWHM of 0.93°. The contribution from the magnetic correlation length at the (001) is 3.62 ± 0.20°. Converting gives 0.13 r.l.u., as shown for base temperature in Fig. 6. This gives a correlation length in real space of $\zeta_T = 90 \pm 10$ Å for the correlation length of the magnetic structure within the plane of the D17 film. As shown in Fig. 6, this correlation length is reduced (increase of the peak width to ~0.45 r.l.u.) such that at the highest temperatures $T_N + 5$ K it extends only to 25% of this value, i.e., ~20 Å.

However, in the case of sample D18 the additional broadening of the (001) above T_N, assuming the intrinsic mosaic is ~0.10°, which is close to that of the substrate, corresponds to ~0.015 r.l.u., so that the magnetic correlation length is some 30 times longer, ~600 Å close to T_N. The striking result is that the physics of the magnetic diffuse scattering

is on substantially different length scales depending on the substrates used and the resulting film quality.

IV. DETERMINATION OF THE THICKNESS AND POSITION OF THE ORDERED AF REGIONS

The absorption coefficient (μ) of UO_2 at the M_4 resonant energy (3.726 keV) (Ref. 26) is approximately 5×10^4 cm^{-1}, so that self-absorption effects are extremely important when passing over the resonant energy. The absorption length $1/\mu = 0.2$ μm $= 2000$ Å. When the x-ray beam enters a crystal for a specular reflection, the effective (or optical) path length is given by $t_{\text{eff}} = t/\sin\theta$, where t is the film thickness and θ is the Bragg angle for the reflection. If the UO_2 film is 1000 Å thick, then t_{eff} for the (001) magnetic reflection is 3276 Å, i.e., longer than the absorption length, and the beam would be attenuated by a factor of ~5. As the energy moves away from this sharp resonance condition, the absorption rapidly decreases so that there is a competition between the diffracted magnetic intensity, which has its peak at the top of the resonance, and the change in absorption. The result of a scan in energy over the resonance of a thick film thus results in a peak with an artificially broad energy width, where we define the half-width at half-maximum (HWHM) as ΔE. For experiments at the actinide M edges, it has long been known that the maximum resonance intensity coincides with the peak of the absorption, so we can treat the broadening of the resonance quantitatively. Typical ΔE values in *bulk* samples in the literature are between 5 and 7 eV. (Recall that most publications give the full-width at half-maximum (FWHM) so that FWHM $= 2 \times$ HWHM.) The advantage of using the HWHM is that it may be compared directly to the lifetime of the core-hole excitation $1/\Gamma$, and for M edge ($3d - 5f$) excitations $1/\Gamma \sim 2$ eV. Both effects can usually be treated adequately with Lorentzian profiles. In considering these effects, Bernhoeft[27] pointed out another important parameter due to the *coherence* of photon beams from synchrotron sources. This is due to the fact that normal scattering theory assumes that the absorption length is much greater than the longitudinal coherence length of photons $= \lambda/(\Delta\lambda/\lambda) \sim 3$ μm. At the U M_4 resonant energy with a third-generation synchrotron source, this assumption is no longer justified, and we saw above that the absorption length is in fact only 0.2 μm, some 15 times less than the coherence length. Bernhoeft[27] derived the necessary expressions and these were tested in a series of experiments at the ESRF by measuring the magnetic scattering from thin films of UPd_2Al_3.[28]

An important conclusion is that for films in the region 300–3000 Å, we expect to see a progressive change in the energy width ΔE, reflecting the competition between absorption (which makes ΔE larger) and the magnetic resonance (which makes ΔE smaller), as demonstrated for films of UPd_2Al_3.[28] We have followed this approach in measuring the scattering intensity as a function of energy over the M_4 resonant energy and then determining the half-width of such scattering intensity. Representative energy scans and simulations are shown in Fig. 8.

The energy scans for the D11 (244 Å) and D17 (4500 Å) samples are shown in Fig. 8(a). The first film (D11) has a narrow width, as expected because self-absorption effects are small. The HWFM is 1.94(9) eV, which is even less than the core-hole lifetime used (2.2 eV) in the calculations of Bernhoeft.[27] As shown in Table II, the uncapped film (D14) also gives a narrow E width, 1.85(9) eV, so we fix the core-hole lifetime to the average of these two values, i.e., $\Delta E_{\text{min}} = 1.9$ eV, establishing the minimum of the so-called Bernhoeft curve.[27] Before making the calculation for the whole curve, we need also the maximum value. For this, we take $\Delta E_{\text{max}} = 4.5(1)$ eV as measured on the same instrument (I16) directly after our experiments on the (003) specular reflection from a

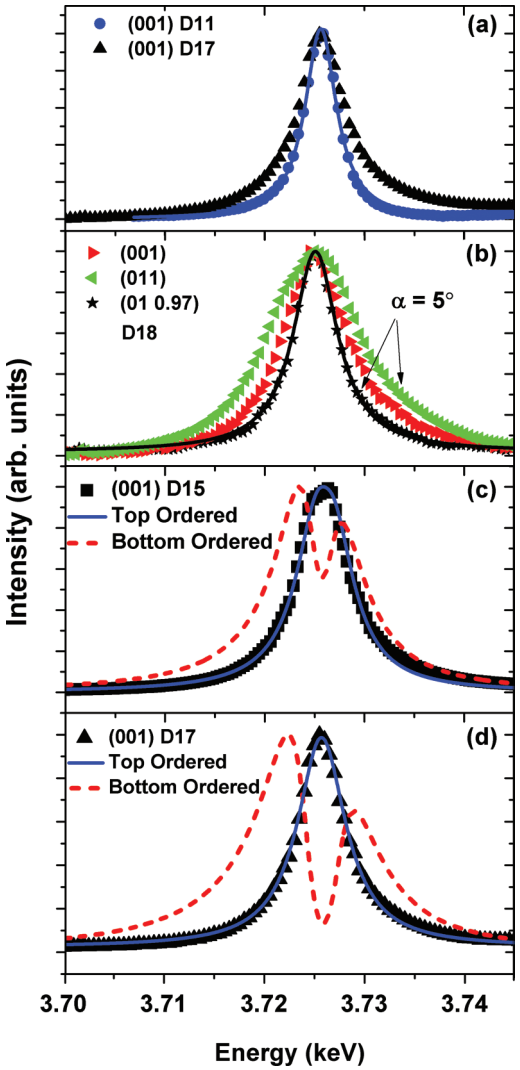

FIG. 8. (Color online) (a) Energy profiles of specular (001) of samples D11 and D17. (b) Energy profiles measured on D18 sample of the specular (001) and off-specular (011). The of-specular (011) and (0 1 0.97) were measured at grazing incidence geometry with $\alpha = 5°$. In both panels, Lorentzian fits are shown to the narrowest spectra. (c) Data (blue points) from D15 (2250 Å) with a simulation of the HWHM = 3 eV as if an AF ordered layer of 600 Å is at the top of the UO_2 film. Red dashed line, simulation with AF-ordered region below a magnetically dead layer of 1650 Å. The HWHM is then ~5.2 eV. (d) As in (c) but with sample D17 of 4500 Å. Blue points are data. Blue line is simulation with 3 eV HWHM. Red dashed line is simulation with AF region of 600 Å below a dead layer of 3900 Å. HWHM of this simulation is ~6.5 eV.

TABLE II. Values related to the study of antiferromagnetism of UO_2 films. See Table I for further details of the films, all of which, except the last entry, are on $LaAlO_3$ substrates. T_N is the Néel temperature (± 0.5 K), β_{AFM} is the critical exponent related to the growth of the AF intensity below T_N as analyzed with $I(T)/I(T_0) \approx (1 - T/T_N)^{2\beta}$ [where $I(T_0)$ is the intensity at base temperature, and where the error bar in β is ± 0.02], ΔE is the half-width at half-maximum of the energy scans through the magnetic peak, and the AFM thickness (t_{AF}) is determined by fitting ΔE to the simulations in Fig. 9. The sample D14 is not capped. The (001) was not measured for sample D11. The last two columns refer to the FWHM in degrees (± 0.10) as measured for the charge (002) and magnetic (001) reflections.

Sample	t (Å)	T_N (K)	$\beta_{AFM}(001)$	$\beta_{AFM}(102)$	$\Delta E(001)$ (eV)	t_{AF} (Å)	$\Delta\omega(002)$ (deg)	$\Delta\omega(001)$ (deg)
D11	244	30.8		0.14	1.94(9)	<150	1.3	
D12	480	30.6	0.22	0.23	2.97(11)	470	1.1	0.9
D13	580	30.4	0.33	0.19	2.31(15)	300	1.0	1.7
D14	1250	30.4	0.33	0.17	1.85(9)	<150	0.9	2.2
D15	2250	30.3	0.31	0.21	2.92(19)	500	0.9	2.1
D17	4500	30.7	0.43		3.04(15)	580	0.9	3.7
D18	2000	26.6	0.56		4.12(9)	~2000		0.16

bulk (i.e., infinitely thick) single crystal of USb tuned to the U M_4 edge. This single crystal had a mosaic width of 0.08°, similar to the D18 sample, and the beam optics are in the same configuration as used for our UO_2 thin films.[29] We find that I16 (Diamond) has slightly better energy resolution than observed at the former ID20 beamline (ESRF),[25] which is also consistent with the minimum values being smaller in these studies than found in the UPd_2Al_3 films of 2.2 eV (Ref. 28) performed at ID20 (ESRF). In the earlier studies,[28] $\Delta E_{max} = 5.0$ eV for a bulk sample, so this is slightly larger than we determined on I16. With these two limits, the Bernhoeft plot[27] for UO_2 can be made; see Fig. 9.

The film D17 of 4500 Å in Fig. 8(a) should show a much broader ΔE but instead has a value of 3.04(15) eV. Moreover, it can be seen in Table II that all the samples based on $LaAlO_3$ substrates have $\Delta E \leqslant 3$ eV. We draw the unexpected conclusion from these measurements that none of the films is magnetically ordered for more than ~600 Å. However, the fact that *all* samples grown on $LaAlO_3$ have T_N 30.5 K is a strong indication that at least those parts that are magnetic are close to stoichiometric $UO_{2.00}$. We shall discuss further below how we can establish the location of this ordered AF region within the thicker films. The surprising result above was the motivation for growing the last sample D18, a UO_2 film of about 2000 Å on a CaF_2 substrate, where the strain is much less and, as we have seen, the UO_2 film quality is much better than when using $LaAlO_3$ substrates. The HWHM of this film (Table II) is 4.12(9) eV. When placed on the Bernhoeft curve in Fig. 9, this gives a formal value of ~1600 Å for D18, but it is clear that as the width falls near the saturated value of Fig. 9, there is considerable error in estimating the ordered region, and we assume it is ordered throughout the film. Furthermore, the JT reflections were strong from this film, again consistent with complete AF ordering. To further confirm the validity of the Bernhoeft curve, we made a number of different experiments with film D18. They are exhibited in Fig. 8(b). The red data points are from the (001) specular reflection, as already mentioned. The green data points are from the (011) nonspecular reflection at 5° incident to the surface, and the black data points are from the same reflection, also with $\alpha = 5°$, but offset from the Bragg point along the truncation rod[12,13] to the position (0 1 0.97). The data taken at the (011) position have an energy width HWHM = 5.8(2) eV, which is even greater than ΔE_{max}. However, with grazing incidence geometry one has to take into account Fresnel effects. Watson *et al.*[13] discusses such effects—see Fig. 6 of that paper. The energy width of the (011) is large—the optical path is also long, about a factor 9 more than the film thickness. We then move away from the magnetic Bragg peak on the so-called magnetic truncation rod. In this geometry, the termination of the surface is the (001) plane, so the magnetic truncation rods[12] are parallel to the [001] axis. It is well known[12,13] that as one moves away from the Bragg position along a truncation rod, the scattering becomes more sensitive to the surface. This can be demonstrated elegantly by observing the energy width as a function of the truncation rod index L. The narrowest plot in Fig. 8(b) is an energy scan taken at the position (0 1 0.97), also with $\alpha = 5°$, and it has a HWHM = 2.5(1) eV. This represents a reduction of ~60% in width compared to that observed at the magnetic Bragg peak. As a rough guide, this corresponds to the top 100–200 Å of the film. This is a vivid demonstration,

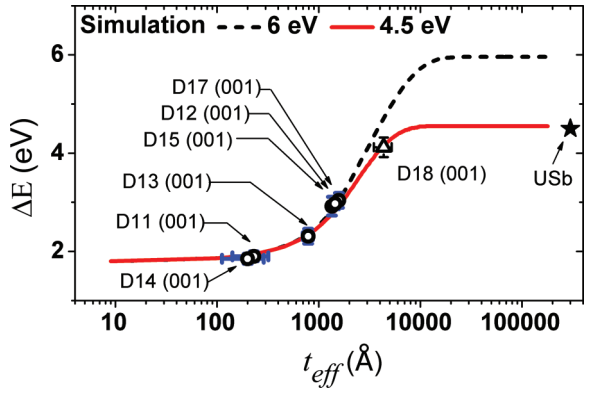

FIG. 9. (Color online) Numerical simulation of the change of the energy width (HWHM) as a function of the effective film thickness, t_{eff}, over the U M_4 resonance. The curve assumes a minimum thickness corresponding to the core-hole lifetime of $\Delta E_{min} = 1.9$ eV, and a $\Delta E_{max} = 4.5$ eV compatible with the results at I16 on a bulk single crystal of USb (see text). The curve traces the expected HWHM vs t_{eff} for specular reflections, where $t_{eff} = t/\sin\theta$, with t the film thickness and θ the Bragg angle.

albeit somewhat qualitative, of the power of this formalism when applied at the U M_4 resonant energy to understand the location of the magnetic scattering volume within a sample. We have therefore tested the Bernhoeft approach with the better film (sample D18), and this allows us to determine the approximate film thicknesses from the HWHMs of the specular (001) reflections of the $LaAlO_3$-based films; these values are shown in Table II.

Furthermore, for the thicker films ($t > 1000$ Å) we can also suggest the location of the ordered region. The principle of this determination is simple, and already discussed by Bernhoeft.[27] If we assume that the films are uniform in the in-plane direction, then the AF region must either be at the top of the film or at the bottom next to the substrate. In the latter case, there will be a dead layer of UO_2 on top that will not contribute to the magnetic intensity, but such a dead layer will absorb the ingoing and outgoing photon beams. This will not be the case if the AF layer is at the top and the dead layer below. Figures 8(c) and 8(d) illustrate with simulations the differences; first (c) with the D15 (2250 Å) samples, and second (d) with the D17 (4500 Å) samples. These simulations were performed with an energy resolution of zero; in practice, the energy resolution is between 0.5 and 1 eV, so the dip in the dashed curves will be smeared out (but not eliminated entirely) in the experiment. The curves in both cases provide strong evidence that the AF ordering (∼600 Å) occurs at the top of the film *with the dead layer on the bottom* next to the substrate, and hence not contributing to the absorption. In addition to the dip in the simulated curve in each case when the dead layer is on top of the film, the curves are considerably broader in their energy width than when the dead layer is below.

Based on the sensitivity of the simulations in Figs. 8(c) and 8(d), we can conclude that for thicknesses of $>\sim$1000 Å the UO_2 orders magnetically at the top of the film, above a magnetically "dead" layer. Of course, of this "dead" layer we can say only that it does not have the antiferromagnetic structure of bulk UO_2. If it had a *different* magnetic structure, the present experiments might not observe it.

V. DISCUSSION AND CONCLUSIONS

We have prepared and characterized thin epitaxial films (250–4500 Å) of UO_2 on $LaAlO_3$ substrates; in addition, we have prepared a ∼2000 Å UO_2 film on a substrate of CaF_2. With the first set of films, we have performed a detailed characterization with *in situ* UPS/XPS to assure stoichiometry. *Ex situ* studies have used x-ray reflectivity, high-angle, and off-specular x-ray diffraction, TEM, and SEM. Because the UO_2 films based on $LaAlO_3$ substrates are in compressive strain (−2%) from the substrate, the UO_2 films are not cubic but have a small tetragonal deformation. The most critical aspect of these films is that they have a large mosaic, which is determined by x-ray rocking curves, and give at best a value of 1°. We ascribe this to being caused by the ferroelastic distortion [560 °C (Ref. 21)] in $LaAlO_3$ through which the films and substrates pass after deposition at high temperature (∼650 °C). We should emphasize that our $UO_2/LaAlO_3$ films are as good as any others grown on either sapphire- or perovskite-based substrates.[6–8] This mosaic of about 1° (see Table I) is to be compared with that of the substrate of $< 0.10°$. In contrast, the UO_2/CaF_2 film (D18) has an exceedingly good mosaic from the magnetic scattering of 0.16°, almost as good as the substrate.

The antiferromagnetic properties have been studied by resonant x-ray scattering using the large enhancement at the U M_4 edge (3.726 keV). All samples, even one uncapped (D14), order antiferromagnetically with the same AF structure as bulk UO_2, and the same T_N. The small reduction in T_N for the UO_2/CaF_2 sample (D18) is almost certainly due to nonstoichiometry of this UO_2 film. AF scattering from as little as 250 Å can be observed.

Whereas the ordering is strongly first-order (i.e., discontinuous) in bulk UO_2 ($\beta = 0$), the behavior in thin films is different. The thinnest films have values of $\beta \sim 0.2$, whereas for the thicker film we find values of $\beta > 0.5$. The difference is well illustrated by the fact that for a specular reflection (001) of the D18 sample (2000 Å UO_2/CaF_2), $\beta_{\mathrm{AFM}} = 0.56(2)$, whereas for the off-specular (011) with the incident beam just 5° from the surface, $\beta_{\mathrm{AFM}} = 0.39(2)$, a significant difference. These two values are measured from the same film, but in one case the beam probes the whole film of 2000 Å, whereas in the other only the top ∼500 Å. In the study of the surface of a bulk crystal, Watson *et al.*[13] showed that the β values increase as one moves away from the reciprocal-lattice point (Fig. 11 of that reference). Since moving away from a reciprocal-lattice point makes the experiment more sensitive to the surface, this suggests a larger β for the surface layers of the crystal. We do not find the same behavior for the films. Instead, β decreases as the film thickness decreases. This would appear to be the opposite tendency as found for the surface of a bulk sample, but one must remember that the latter are influenced by the interaction between the surface layer and the bulk, which is absent in thin films. This would appear to be an area in which some theoretical guidance would be useful.

Jahn-Teller-like distortions of the oxygen cage were observed easily from sample D18, but they were harder to observe in the $LaAlO_3$-based films. This could be because if the film has tetragonal symmetry the JT distortion does not exist, or because the distortion from much less than ∼500 Å is hard to observe. The JT effect is a secondary one, induced by the magnetic order, which is shown clearly by the fact that $\beta_{\mathrm{JT}} \sim 2\beta_{\mathrm{AFM}}$ (Fig. 5). No diffuse charge scattering is associated with the JT transition, which is not surprising as it is small and a second-order effect.

An important observation is the strong diffuse scattering found only in the films based on $LaAlO_3$ substrates (Figs. 5 and 6). Such scattering is strongly anisotropic, essentially confined to the plane perpendicular to the growth axis. It is readily observable and continues to at least $T_N + 5$ K. Because such diffuse scattering is absent in the UO_2/CaF_2 film (Fig. 7), it is not an intrinsic feature of the disordering of the moments in epitaxial UO_2. Instead, the scattering must represent a second length scale associated with the strain within the samples, and the resulting structural inhomogeneity. Such effects were already observed in a UO_2 single crystal that was intentionally roughened[11] (see Figs. 12 and 13 of that paper) and was also observed in Ho films[30] (see Fig. 2 of that reference). In high-quality films, such as the UO_2/CaF_2 sample (D18),

the critical fluctuations are small and almost isotropic [see Fig. 7(b)].

The majority of studies on the second-length scale effect[31,32] have found that the additional scattering from defects in the surface region gives rise to scattering that is narrower in reciprocal space than that found for the pure material. This is also the case of a roughened UO_2 surface.[11] In our case, both the $LaAlO_3$- and CaF_2-based films indeed show critical fluctuations on a longer length scale (i.e., narrower in reciprocal space) than found intrinsically for UO_2 (see Fig. 13 of Ref. 11), where the fluctuations are on a short length scale of no more than 5–10 Å and show little anisotropy. However, the effects in the different films show different length scales, as well as anisotropy in one case, and almost none in the other. This clearly shows the drastic effects of strain and/or of poorer crystallinity in the $LaAlO_3$-based samples. One interesting observation is that in each case there is a change in the transverse correlation length by about a factor of 4. Compare, for example, the change in the transverse widths in Figs. 5, 6, and 7. In each case, the increase of the transverse width above T_N corresponds to about four times the width at base temperature, even though the latter are different for the three samples investigated.

To enter into a detailed analysis of this unusual diffuse magnetic scattering, we would require more samples and a better quantitative understanding of the influence of the interfaces between substrate and film and the microscopic strain; for this paper, we confine ourselves to qualitative remarks on this observed magnetic diffuse scattering.

The most unexpected result in this study was when the formalism of Refs. 26 and 27 was applied to the width of the energy scan across the resonant value. We show that the thicker films of $UO_2/LaAlO_3$ are not fully ordered. In fact, we are unable to induce AF magnetic ordering greater than ~600 Å, even if the total width of the film is 4500 Å. A further surprise, which is illustrated forcibly in Figs. 8(c) and 8(d), is that the AF-ordered layer within the film is almost certainly at *the top of the film*. The dead magnetic layer must be placed *below* the film (i.e., adjacent to the substrate) rather than *vice versa*. The simulations in Figs. 8(c) and 8(d) show a dip near the absorption edge and a major broadening of the energy widths for increasing film thickness. Such effects are *not* observed experimentally.

Why should the dead magnetic UO_2 layer be adjacent to the film-substrate interface? Obviously, this is a difficult question, and there may be alternative answers. Perhaps a clue can be seen in the FWHM mosaic values given for the (002) charge and (001) magnetic reflections in Table II. Here we observe that the thicker films have progressively larger magnetic mosaic widths (last column in Table II). As discussed earlier, we associate these increasing widths with a *decreasing magnetic correlation length* in the thicker films. The tetragonal nature of UO_2 observed in all the $LaAlO_3$-based films (Fig. 3) gives one possible explanation for partial ordering of these films. We propose that tetragonally distorted UO_2 is nonmagnetic. The special triple-**k** ordering of bulk UO_2 should be emphasized; bulk UO_2 remains cubic below T_N.[10] The interactions that stabilize this magnetic structure may well be different if the crystal structure is tetragonal.

For thin UO_2 films, for example D12 (480 Å), the relative orientation of the crystalline blocks [see Fig. 4(b)] is more diverse [corresponding to a *larger mosaic* of the charge (002) for thinner films] than for the thicker films, so that even if the average tetragonality (see Fig. 3) is larger than for thicker films, it may be easier for the UO_2 film to adjust to the strains and the magnetic regions may be cubic, as in bulk UO_2. They then order magnetically with intensity at the (001) reflection. For thicker films, however, the mosaic structure is better [smaller mosaic of the (002) reflection in Table II] so that the tetragonal distortion is more robust. If this distortion is present in the layers of UO_2 adjacent to the substrate, this might explain why such layers do not order with intensity at the (001) reflection. As we proceed through such dead layers, the tetragonal distortion may relax, leading to the short-range magnetic ordering [larger mosaic of the magnetic (001) reflection in Table II] for the thicker films. Of course, the dead layers may order below 12 K, or even with another ordering wave vector—this aspect would be hard to establish, but it remains an intriguing possibility.

Another possibility is a distribution of oxygen stoichiometry as a function of thickness of the UO_2 film. However, such a model has difficulty explaining why the $LaAlO_3$-based films all have much the same T_N (see Table II).

These unusual effects do not appear in the D18 sample of UO_2/CaF_2, where, to the best of our knowledge, the whole film orders with the same magnetic structure as found in bulk UO_2. However, the match between UO_2 and CaF_2 is excellent, so we would not expect any complications as found (unexpectedly) in the work with $LaAlO_3$-based films. It will also be interesting to examine UO_2 films grown on YSZ (ytrria-stabilized zirconia), in which Strehle *et al.*[8] found narrow mosaic widths.

ACKNOWLEDGMENTS

We acknowledge the efforts of Rob Walton to implement the software to perform truncation rod scans at I16 (Diamond), and discussions with Steve Collins at the beamline.

*Present address: ISIS, Rutherford Appleton Laboratory, Harwell Science and Innovation Campus, Oxon OX11 0QX, United Kingdom.

[1]H. Idriss, Surf. Sci. Rep. **65**, 67 (2010).

[2]S. van den Berghe, F. Miserque, T. Gouder, B. Gaudreau, and M. Verwerft, J. Nucl. Mater. **294**, 168 (2001).

[3]F. Miserque, T. Gouder, D. H. Wegen, and P. D. W. Bottomley, J. Nucl. Mater. **298**, 280 (2001).

[4]Q. Chen, X. Lai, B. Bai, and M. Chu, Appl. Surf. Sci. **256**, 3047 (2010).

[5]A. Seibert, D. H. Wegen, T. Gouder, J. Römer, T. Wiss, and J.-P. Glatz, J. Nucl. Mater. **419**, 112 (2011).

[6]A. K. Burrell, T. M. McCleskey, P. Shukla, H. Wang, T. Durakiewicz, D. P. Moore, C. G. Olson, J. J. Joyce, and Q. Jia, Adv. Mater. **19**, 3559 (2007).

[7]R. Temple and R. C. C. Ward, internal report, University of Oxford, UK (2010).
[8]M. M. Strehle, B. J. Heuser, M. S. Elbakhshwan, X. Han, D. J. Gennardo, H. K. Pappas, and H. Ju, Thin Solid Films **520**, 5616 (2012).
[9]H. Y. Hwang, Y. Isawa, M. Kawasaki, B. Keimer, N. Nagaosa, and Y. Tokura, Nat. Mater. **11**, 103 (2012).
[10]P. Santini, S. Carretta, G. Amoretti, R. Caciuffo, N. Magnani, and G. H. Lander, Rev. Mod. Phys. **81**, 807 (2009).
[11]G. M. Watson, B. D. Gaulin, D. Gibbs, T. R. Thurston, P. J. Simpson, S. M. Shapiro, G. H. Lander, H. Matzke, S. Wang, and M. Dudley, Phys. Rev. B **53**, 686 (1996).
[12]G. M. Watson, D. Gibbs, G. H. Lander, B. D. Gaulin, L. E. Berman, H. Matzke, and W. Ellis, Phys. Rev. Lett. **77**, 751 (1996).
[13]G. M. Watson, D. Gibbs, G. H. Lander, B. D. Gaulin, L. E. Berman, H. Matzke, and W. Ellis, Phys. Rev. B **61**, 8966 (2000).
[14]R. C. C. Ward, R. A. Cowley, N. Ling, W. Goetze, G. H. Lander, and W. G. Stirling, J. Phys.: Condens. Matter **20**, 135003 (2008).
[15]T. Gouder, J. Electron. Spectrosc. Relat. Phenom. **101–103**, 419 (1999).
[16]M. A. Moran and M. E. Vickers, Rep. Prog. Phys. **72**, 036502 (2009).
[17]A. Gibaud, R. A. Cowley, D. F. McMorrow, R. C. C. Ward, and M. R. Wells, Phys. Rev. B **48**, 14463 (1993).
[18]A. Wildes, J. Mayer, and K. Theis-Bröhl, Thin Solid Films **401**, 7 (2001).
[19]B. Wölfing, K. Theis-Bröhl, C. Sutter, and H. Zabel, J. Phys.: Condens. Matter **11**, 2669 (1999).
[20]O. Durand, A. Letoublon, D. J. Rogers, and F. H. Teherani, Thin Solid Films **519**, 6369 (2011).
[21]S. Bueble, K. Knorr, E. Brecht, and W. W. Schmahl, Surf. Sci. **400**, 345 (1998).
[22]A. G. Lehmann, C. Sanna, N. Lampis, F. Congiu, G. Concas, L. Maritato, C. Aruta, and A. Y. Petrov, Eur. Phys. J. B **55**, 337 (2007).
[23]S. B. Wilkins, R. Caciuffo, C. Detlefs, J. Rebizant, E. Colineau, F. Wastin, and G. H. Lander, Phys. Rev. B **73**, 060406(R) (2006).
[24]J. Faber, G. H. Lander, and B. R. Cooper, Phys. Rev. Lett. **35**, 1770 (1975).
[25]L. Paolasini, C. Detlefs, C. Mazzoli, S. Wilkins, P. P. Deen, A. Bombardi, N. Kernavanois, F. de Bergevin, F. Yakhou, J. P. Valade *et al*., J. Synch. Radiat. **14**, 301 (2007).
[26]J. O. Cross, M. Newville, J. J. Rehr, L. B. Sorensen, C. E. Bouldin, G. Watson, T. Gouder, G. H. Lander, and M. I. Bell, Phys. Rev. B **58**, 11215 (1998).
[27]N. Bernhoeft, Acta Crystallogr. Sect. A **55**, 274 (1999).
[28]N. Bernhoeft, A. Hiess, S. Langridge, A. Stunault, D. Wermeille, C. Vettier, G. H. Lander, M. Huth, M. Jourdan, and H. Adrian, Phys. Rev. Lett. **81**, 3419 (1998).
[29]J. Lim (private communication).
[30]S. Konings, C. Schüßler-Langeheine, H. Ott, E. Weschke, E. Schierle, H. Zabel, and J. B. Goedkoop, Phys. Rev. Lett. **106**, 077402 (2011).
[31]P. M. Gehring, K. Hirota, C. F. Majkrzak, and G. Shirane, Phys. Rev. Lett. **71**, 1087 (1993).
[32]M. Altarelli, M. D. Nunez-Regueiro, and M. Papoular, Phys. Rev. Lett. **74**, 3840 (1995).